Dark matter decay to neutrinos

Carlos A. Argüelles,[1] Diyaselis Delgado,[1,*] Avi Friedlander,[2,3] Ali Kheirandish,[4,5] Ibrahim Safa,[6,7,1]
Aaron C. Vincent,[2,3,8] and Henry White[2,3]

[1]*Department of Physics and Laboratory for Particle Physics and Cosmology, Harvard University,
Cambridge, Massachusetts 02138, USA*
[2]*Department of Physics, Engineering Physics and Astronomy, Queen's University,
Kingston, Ontario K7L 3N6, Canada*
[3]*Arthur B. McDonald Canadian Astroparticle Physics Research Institute,
Kingston, Ontario K7L 3N6, Canada*
[4]*Department of Physics and Astronomy, University of Nevada, Las Vegas, Nevada, 89154, USA*
[5]*Nevada Center for Astrophysics, University of Nevada, Las Vegas, Nevada 89154, USA*
[6]*Department of Physics, Columbia University, New York, New York 10027, USA*
[7]*Department of Physics and Wisconsin IceCube Particle Astrophysics Center, University of Wisconsin,
Madison, Wisconsin 53706, USA*
[8]*Perimeter Institute for Theoretical Physics, Waterloo, Ontario N2L 2Y5, Canada*

It is possible that the strongest interactions between dark matter and the Standard Model occur via the neutrino sector. Unlike gamma rays and charged particles, neutrinos provide a unique avenue to probe for astrophysical sources of dark matter, since they arrive unimpeded and undeflected from their sources. Previously, we reported on annihilations of dark matter to neutrinos; here, we review constraints on the decay of dark matter into neutrinos over a range of dark matter masses from MeV to ZeV, compiling previously reported limits, exploring new electroweak corrections and computing constraints where none have been computed before. We examine the expected contributions to the neutrino flux at current and upcoming neutrino experiments as well as photons from electroweak emissions expected at gamma-ray telescopes, leading to constraints on the dark matter decay lifetime, which ranges from $\tau \sim 1.2 \times 10^{21}$ s at 10 MeV to 1.5×10^{29} s at 1 PeV.

I. INTRODUCTION

The angular power spectrum of the cosmic microwave background (CMB) as well as the matter distribution on large scales, the clustering of galaxies, and the measured kinematics of stars and gas within those galaxies all point to a large component of weakly-interacting *dark matter* (DM), constituting 85% of all matter in the Universe [1,2]. While these observations imply an equation of state consistent with a cold, collisionless fluid, no microphysical connection has yet been found between DM and the Standard Model (SM) of particle physics. Numerical coincidences such as the one-to-five ratio of dark-to-ordinary matter sustain our hope that DM decoupled late enough in the history of the Universe to require a coupling well below the

Planck scale and thus be describable in the language of particle physics.

The parameter space of such nongravitational interactions is immense, and myriad portals are potentially available. Traditional searches for electroweak and supersymmetry-inspired WIMPs in the GeV-TeV mass range that scatter with or annihilate to quarks have expanded in the past decades to encompass light axionlike [3] and minicharged particles [4–8], sub-GeV nonthermal DM candidates [9,10], primordial black holes [11], and other exotic objects. In some of these scenarios, dark matter can be unstable and decay to Standard Model particles.

Direct searches for such DM rely on elastic scattering with electrons or nuclei, while indirect searches look for signatures of decay or annihilation into SM particles. Products of DM decay (or annihilation) into SM particles eventually create a flux of stable particles, i.e., protons, electrons, photons, or neutrinos. Here, we focus on the latter. A direct neutrino portal would render direct detection impracticable, and indirect detection very difficult, owing to the minuscule cross section of neutrinos at low energies. However, at high energies, the neutrino cross section grows

---

*Corresponding author: ddelgado@g.harvard.edu

and is no longer suppressed by the mass of the heavy bosons but by the momentum transfer as is the case of photon-nucleon interactions [12–14]. Additionally, high-energy gamma rays can be attenuated as they travel from their sources of production to Earth, while neutrinos voyage unimpeded. Therefore, the study of neutrinos represents a final frontier in the search for indirect signatures of DM. The study of this channel is further motivated by connections between the dark sector and neutrinos. These have been proposed in a variety of different contexts, including the scotogenic scenarios where neutrinos gain their mass via interacting with the dark sector [15–21], the Majoron scenario [22], or see-saw models [23]. In many of these models, UV physics can destabilize the DM, leading to a decay to $\bar{\nu}\nu$, which may dominate over other channels. These models have motivated numerous dedicated studies, mainly in the context of discovering heavy DM using neutrino line searches [24–35], and many neutrino experiments have hunted for DM signatures in their observations [36–42], so far yielding null results.

Previously, we presented an updated compendium of constraints on particle DM annihilation to neutrinos [43]. Here, we turn our attention to the production of neutrinos from DM decay, directing special attention to the higher-mass region. At masses greater than $\sim$TeV, electroweak (EW) corrections can "decloak" the DM, producing high-energy photons, even when directly decaying to neutrinos that can be detectable at current and future gamma-ray observatories [44]. We thus present limits from current measurements and sensitivities for upcoming experiments covering a DM mass range starting at 20 MeV and spanning well into the ultraheavy domain up to 10^{11} GeV. Although recent LHAASO results are on par with IceCube's recent analyses, we will find that current and future neutrino telescopes retain superior sensitivity across nearly the entire range of masses that we consider. This is due to three factors: the loop suppression of the gamma-ray production rate, the growth of the electroweak cross section with energy, and the loss of high-energy gamma rays to interactions in the interstellar and intergalactic medium.

We begin by briefly describing the signature of DM decaying to neutrinos at both neutrino telescopes and gamma-ray observatories. We present our new results in Sec. III and offer parting words of wisdom in Sec. IV.

II. DARK MATTER DECAYS TO NEUTRINOS

The expected flux per neutrino flavor at Earth from decay of DM with mass m_χ and lifetime τ_χ is

$$\frac{d\Phi_{\nu+\bar{\nu}}}{dE_\nu} = \frac{1}{4\pi}\frac{1}{\tau_\chi m_\chi}\frac{1}{3}\frac{dN_\nu}{dE_\nu}D(\Omega). \qquad (1)$$

Below the electroweak scale, the neutrino spectrum per decay is $dN_\nu/dE_\nu = 2\delta(1 - 2E/m_\chi)m_\chi/2E^2$; at higher masses a low-energy tail arises as discussed in Ref. [44].

Because relevant backgrounds follow a power-law distribution, only the delta contribution is relevant for neutrino constraints. The so-called D-factor, $D(\Omega)$, is an integral of the DM distribution $\rho(x)$ along the line of sight and solid angle $\Delta\Omega$:

$$D \equiv \int d\Omega \int_{\text{l.o.s.}} \rho_\chi(x)dx. \qquad (2)$$

We assume the Galactic DM spatial distribution is modeled by an Navarro-Frenk-White (NFW) profile with a slope parameter $\gamma = 1.2$ and a scale radius $r_s = 20$ kpc, and we set the local DM density to $\rho_0 = 0.4$ GeV cm^{-3}. These parameters are consistent with the results of, e.g., Ref. [45], which point out a strong dependence on how the baryonic potential is modeled. We take the distance to the galactic center to be $R_0 = 8.127$ kpc [46]. Here, we mainly strive to make results as self consistent as possible by using common halo parameters in all of our analyses. We have assumed equal production of each flavor, which leads to equal flavors at Earth. Due to neutrino oscillation, this will remain approximately true regardless of the initial flavor composition.

The D-factor depends on the field of view of each experiment. Effective areas are reported as a function of elevation (or equivalently, zenith angle). Given each experiment's latitude and altitude, we integrate these acceptances over a period of 24 hours, where the solid angle integral is weighted by the fractional acceptance. This defines an effective D-factor:

$$D_{\text{eff}} = \int dt \int d\Omega \int_{\text{l.o.s.}} \rho_\chi(x)F(\Omega, t)dx, \qquad (3)$$

where $F(\Omega, t)$ is the fractional acceptance in equatorial coordinates. This procedure is simplified for experiments at the South Pole (IceCube, ANITA), where elevation and declination are equivalent.

In computing the yield of dark matter in a given experiment, we convolve the experimental efficiency with flux from neutrinos from a given direction. For our background agnostic constraints, the flux obtained by this procedure is then compared to the unfolded neutrino fluxes. When published experimental results on dark matter annihilation use a directional analysis, such as the case of ANTARES, we rescale the result by the efficiency-weighted ratio of the dark matter J to D factors; namely the ratio of expected signal yield in the annihilation to decay scenarios. Efficiencies used for each experiment are given in Appendix Table III.

Based on Eq. (1), we produce limits on the DM decay rate, using results from different analyses of existing data [28,43,47–60] or forecasted sensitivities [61–66]. The full list of neutrino experiments is given in the top section of Table I. We also list the neutrino energy range covered by

TABLE I. Neutrino (top) and gamma-ray (bottom) observatories considered in this work. Here, "All Flavors" denotes both neutrinos and antineutrinos of electron, muon, and tau flavor. The experiments given in *italic* font are upcoming or proposed detectors.

Energy (GeV)	Experiment	Directionality	Particles
$(2.5\text{–}15) \times 10^{-3}$	Borexino [67]	$\times$	$\bar{\nu}_e$
$(8.3\text{–}18.3) \times 10^{-3}$	KamLAND [68]	$\checkmark$	$\bar{\nu}_e$
$(10\text{–}40) \times 10^{-3}$	*JUNO* [69]	$\checkmark$	$\bar{\nu}_e$
$(1.5\text{–}100) \times 10^{-2}$	SK [57]	$\times$	$\bar{\nu}_e$
$0.1\text{–}30$	*DUNE* [70]	$\times$	$\nu_e, \bar{\nu}_e, \nu_\tau, \bar{\nu}_\tau$
$0.1\text{–}30$	*HK* [70]	$\times$	$\nu_e, \bar{\nu}_e, \nu_\tau, \bar{\nu}_\tau$
$1\text{–}10^4$	SK [71,72]	$\checkmark$	All Flavors
$20\text{–}10^4$	IceCube [60]	$\checkmark$	All Flavors
$50\text{–}10^5$	ANTARES [73]	$\checkmark$	$\nu_\mu, \bar{\nu}_\mu$
$10^3\text{–}10^7$	*P-ONE* [74]	$\checkmark$	All Flavors
$10^4\text{–}10^7$	*KM3NeT* [75]	$\checkmark$	All Flavors
$10^6\text{–}10^8$	*TAMBO* [76]	$\checkmark$	$\nu_\tau, \bar{\nu}_\tau$
$>10^7$	*IceCube-Gen2* [77]	$\checkmark$	All Flavors
$>10^8$	*RNO-G* [78]	$\checkmark$	All Flavors
$>10^8$	*GRAND* [47]	$\checkmark$	$\nu_\tau, \bar{\nu}_\tau$
$10^8\text{–}10^{11}$	Auger [79]	$\checkmark$	All Flavors
$10^{-1}\text{–}10^2$	Fermi-LAT [80]		γ
$10^3\text{–}10^9$	*CTA* [81]		γ
$10^4\text{–}10^9$	HAWC [82]		γ
$10^5\text{–}10^9$	LHAASO [83]		γ
$10^6\text{–}10^9$	IceTop [84]		γ
$10^7 - 2 \times 10^9$	KASCADE [85]		γ
$10^8 - 2 \times 10^{10}$	CASA-MIA [86]		γ
$10^9 - 2 \times 10^{12}$	EAS-MSU [87]		γ
$10^{11.5}\text{–}10^{14}$	TA-SD [88]		γ
$>10^{12}$	Auger-SD [89]		γ

each experiment, spanning from 10 MeV at Borexino to $>10^{11}$ GeV at IceCube and AUGER, as well as each experiment's neutrino flavor sensitivity. For a detailed description of each experiment and its sensitivity, we point the reader to Ref. [43]. The D-factors for each experiment are computed by integrating the exposure of each telescope over 24 hours. The resulting exposures and D-factors are tabulated in Table III in the Appendix.

The decay lifetime constraints result from a comparison between the flux sensitivities from each experiment and the expected neutrino flux from DM decay. This approach assumes a branching ratio of 100% of DM decay to neutrinos can describe the total neutrino flux measurements in the Galactic Center region. Our forecasts assume five years of exposure for each of the following experiments: JUNO [69], DUNE [70], Hyper-Kamiokande (HK) [70], RNO-G [78], IceCube-Gen2 [77], KM3NeT [75], P-ONE [74], TAMBO [76], and GRAND [47]. Constraints that are not derived by us, but are reported by experiments or other groups, are rescaled to match the D-factors used in this work. This enables a fair comparison between different experimental constraints.

Data are available at various stages of the analysis pipeline. The closer to event level, the stronger the constraining power. Depending on how data are reported, we are able to compute lifetime limits with varying precision. The methods by which these different datasets are converted into a lower bound on DM lifetime is outlined below. Further, Table II outlines the type of data used to calculate all lifetime limits within this work. Below we discuss the approach applied to each individual dataset according to the exposure time and neutrino flavor detected by the experiment.

The full list of references for each experiment is provided in Table I.

(1) *Lifetime limit*

  Constraints labeled IceCube (Bhattacharya) are based on Ref. [28]. They performed an event-level calculation of limits on dark matter decay and annihilation. They present separate constraints for decays to electron, mu, and tau flavor. We take the least constraining (most conservative) limit for each energy bin, and divide by three to account for our assumption of equal decay to all flavors. These limits

were not scaled by the ratio of D factors due to matching NFW halo profile assumptions.

Similarly, for the sensitivities of JUNO, based on Ref. [62], the D-factor definition matches the halo parameters used for this analysis and does not require rescaling.

(2) *Rescaled annihilation cross section limits*

A number of experiments have presented constraints on dark matter annihilation cross section $\langle \sigma v \rangle$, but not decay. These annihilation limits can be converted into a limit on DM lifetime by rescaling by the appropriate ratio of D-factor to J-factor, i.e.,

$$\tau_\chi^{\text{limit}} = \frac{2m_\chi}{DJ\langle \sigma v \rangle^{\text{limit}}}. \tag{4}$$

Note that the J-factor refers to the annihilation equivalent of Eq. (2) with ρ_χ^2.

This is done for IceCube, IceCube-DeepCore, and SuperKamiokande. This procedure is used for sensitivity forecasts for DUNE, HyperKamiokande, and KM3NeT. For our ANTARES constraint, based on [90], effective areas were presented in Ref. [104] for three different nadir angle bins, as a function of neutrino energy. This allows us to perform a more accurate rescaling of the effective $\langle \sigma v \rangle$ to τ_χ conversion, by combining Eqs. (3) and (4) to take into account the acceptance for each mass for a given time of day.

(3) *Upper limit on neutrino flux*

Borexino, KamLand, and SuperKamiokande ($\bar{\nu}_e$ search) have presented energy-binned neutrino flux limits. We translate these to limits on the DM lifetime using Eq. (1). Limits on only neutrinos or antineutrinos were scaled by an additional factor of 2 to translate them to a limit on $\Phi_{\nu+\bar{\nu}}$. These limits are not derived using angular information in the data, and are thus less sensitive than a dedicated analysis.

(4) *Diffuse neutrino flux*

Limits on the diffuse neutrino flux are typically presented under the assumption of a power-law spectrum. We label the size of the logarithmic energy bins, $\Delta \equiv \log_{10} E_i - \log_{10} E_{i+1}$ for the ith bin, and the power law, $E^{-\alpha}$, such that the limit on the diffuse flux can be written as

$$\left.\frac{d\phi}{dE}\right|_{\text{lim}} = f_0 E^{-\alpha}, \tag{5}$$

where f_0 is constant. This first needs to be integrated to turn this limit into a limit on the total flux within each energy bin, and then compared with the integral of Eq. (1) within the bin, for a given m_χ. Schematically,

$$\phi_{\text{lim}}(\bar{E}) = 4\pi \int_{\bar{E}10^{-\Delta/2}}^{\bar{E}10^{+\Delta/2}} f_0 E^{-\alpha} dE. \tag{6}$$

Equating Eq. (6) and the integral of Eq. (1) yields

$$\tau = \frac{2D(\alpha-1)}{3m_\chi^2(4\pi)^2}\left((10^{\Delta/2} - 10^{-\Delta/2})\left.\frac{d\phi}{dE}\right|_{\text{lim}}\right)^{-1} \tag{7}$$

for $\alpha = 1$, and

$$\tau = \frac{2D}{3m_\chi^2(4\pi)^2}\left(\Delta \ln(10)\left.\frac{d\phi}{dE}\right|_{\text{lim}}\right)^{-1} \tag{8}$$

for $\alpha = 2$. Equation (8) was applied for the analyses done on Auger data, SuperKamiokande atmospheric neutrino data, and IceCube atmospheric neutrino data. Equation (7) was applied for GRAND and IceCube HE analyses.

(5) *Projected effective areas*

Finally, some of our projections require a complete derivation of sensitivities. We proceed as in Ref. [43].

For IceCube Gen-2, P-ONE, and TAMBO we assume an atmospheric background [105] $\phi_{\text{atm},0}(E/10^4 \text{ GeV})^{-3.39}$, with $\phi_{\text{atm},0} = 1.1749 \times 10^{-14} \text{ GeV}^{-1} \text{ s}^{-1} \text{ cm}^{-2} \text{ sr}^{-1}$ and a power law astrophysical neutrino flux $\phi_{\text{astro},0}(E/10^5 \text{ GeV})^{-2.28}$, with $\phi_{\text{astro},0} = 1.44 \times 10^{-18} \text{GeV}^{-1}\text{s}^{-1}\text{cm}^{-2}\text{sr}^{-1}$ [106]. We use projected effective areas, presented in elevation bins, from Refs. [65,66,93] respectively for Gen-2, P-ONE, and TAMBO. These are convolved with the expected flux in Eq. (3). We derive an upper limit sensitivity based on five years of exposure using a binned Poisson likelihood (see Ref. [43]).

For the lower energies of DUNE and JUNO, we do not have effective areas in terms of the top-of-the-atmosphere neutrino flux. We use the predictions of [107] to model the atmospheric background at SURF, and nuSQuIDS to account for oscillation [108–110]. We focus on e- and τ-flavored charged-current interactions, comparing the expected energy distribution. We do not consider event-by-event directional information. For the charged lepton energy resolution, we assume a fractional resolution of $2\% + 15\%/\sqrt{E/\text{GeV}}$ [111] and assume 100% efficiency.

We assume that charged-current electron-neutrino interactions deposit all their energy in the detector. However, for tau-neutrino charged-current interactions, the visible energy is lower due to invisible neutrinos produced in the prompt τ decay. To reduce the atmospheric neutrino background, which is

mainly contributed by muon-neutrino charged-current processes, we exclude them from the analysis, considering that DUNE morphological identification can effectively identify them.

A. Gamma rays from electroweak corrections

Above the TeV scale, electroweak corrections can lead to the production of photons. These result in two distinct gamma-ray fluxes. First, "prompt" high-energy flux consisting of primary photons emitted during the dark matter decay to neutrinos. Second, lower-energy (GeV–TeV) photon signal due to scattering of primary photons with the CMB and extragalactic background light (EBL). The prompt gamma-ray spectra can be obtained via the HDMSpectra package [44], which solves the Dokshitzer-Gribo-Lipatov-Altarelli-Parisi (DGLAP) equations above the electroweak scale with initial conditions given by the DM decay channel. At the edge of this scale, HDMSpectra matches its solution with PYTHIA 8.2 [112], which calculates the effects of particle showers, hadronization, and light particle decays.

We use the gamma-ray distribution from this package to derive constraints using gamma-ray datasets in a similar way to how we proceed with neutrinos. One important difference is the inclusion of an additional factor of $\exp(-\tau_{\gamma\gamma})$ in Eq. (1). This factor accounts for attenuation due to pair production from scattering of high-energy gamma-rays with the background light [113], for which CMB photons provide the dominant attenuation channel. For the galactic component, we conservatively include this as a constant factor by taking the average attenuation rate over a distance of 10 kpc. We will present limits from *Fermi*-LAT [80], HAWC [82], LHAASO [83], IceTop [84], KASCADE-Grande [85], CASA-MIA [86], EAS-MSU [87], TA-SD [88], and Auger-SD [89] observations as well as a projected sensitivity for CTA [81]. For CTA, we consider the differential sensitivity from [97] and convert it to an upper limit on the total flux per decade of energy, which is defined as the minimum flux required to obtain a 5σ point source detection from CTA Southern array for a total observation time of 50 hours.

In the case of IceTop, we use the differential upper limits at 90% confidence limit (C.L.) reported in [95]. These are then converted to total integrated emission per energy decade. For KASCADE, KASCADE-Grande, CASA-MIA, EAS-MSU, TA-SD, and Auger-SD, we use the integral gamma-ray flux upper limits reported in Refs. [99,102,103,114,115]. For HAWC, we follow the same procedure for the flux upper limit in each declination band [98] and then further select the most stringent constraint among all bands. All integrated gamma-ray fluxes are then compared to the expected total flux from DM decay to neutrinos with the photon spectrum from electroweak corrections. This comparison then yields our constraints on the DM decay lifetime. Limits for

decaying DM to all neutrino flavors from LHAASO were taken from [116].

The experimental upper limits, shown in Fig. 1, are given in terms of the gamma-ray integral flux, which is defined as:

$$\Phi_\gamma(E_\gamma) = \int_{E_\gamma}^\infty d\tilde{E}_\gamma \frac{d\Phi_\gamma}{d\tilde{E}_\gamma} = \int_{E_\gamma}^\infty d\tilde{E}_\gamma \, \Phi_0 \left(\frac{\tilde{E}_\gamma}{E_0}\right)^{-\Gamma}, \quad (9)$$

where the power-law index Γ is conventionally chosen to be 2. The gamma-ray integral flux upper limit is derived by finding the value of Φ_0, such that the 90 C.L. upper limit on the number of detected events matches the number of expected events obtained from the convolution of the detector effective area with the power-law flux. Namely, it saturates the following equation:

$$N_{\text{upper limit}}^{90\%} = \int_{E_\gamma}^\infty d\tilde{E}_\gamma \, \Phi_0^{90\% \text{ u.l.}} \left(\frac{\tilde{E}_\gamma}{E_0}\right)^{-\Gamma} A_{\text{eff}}(E_\gamma) T. \quad (10)$$

At sufficiently large masses, gamma rays produced from decays outside our galaxy can scatter down to produce a signal that is observable at lower energies in experiments such as *Fermi*-LAT. High-energy gamma rays traversing the intergalactic medium (IGM) are absorbed and scattered by photons from the CMB and EBL, attenuating the signal [117]; see Ref. [118] for a recent detailed discussion. Scattering and absorption of gamma rays result in cascades that transform any sufficiently high-energy gamma-ray source into a universal spectrum [119] that peaks within the *Fermi* telescope's sensitivity range. In what follows we take advantage of this universality to extend gamma-ray limits to higher dark matter masses, and convert them to limits on decay to neutrinos.

Reference [120] sets constraints on the lifetime of DM decay to SM particles using *Fermi* observations of the isotropic gamma-ray background. We use the limits presented there for DM decays to neutrino pairs that extend up to $m_\chi = 10^7$ GeV. The limits presented in Ref. [120] constrain the channel $\chi \to \bar{b}b$ up to 10^{10} GeV. We use these to obtain corresponding limits in the channel of interest, DM decay to neutrino pairs. The idea of the *universal spectrum* means that regardless of the initial gamma-ray spectral shape, the spectrum arriving at Earth is universal. Therefore limits on dark matter decay to neutrinos are related to the $\chi \to \bar{b}b$ limits by a factor of $F_{\chi\to\bar{\nu}\nu}^\gamma / F_{\chi\to\bar{b}b}^\gamma = 0.06$, where $F_{\chi\to\bar{X}X}^\gamma$ is the fraction of energy per decay to species X going into photons. Appendix Fig. 4 shows that this rescaling yields the published $\bar{\nu}\nu$ results below 10^7 to a reasonable accuracy, allowing us to confidently extend these limits up to 10^{10} GeV. We find that the *Fermi*-LAT constraints remain subdominant over the full range of masses considered.
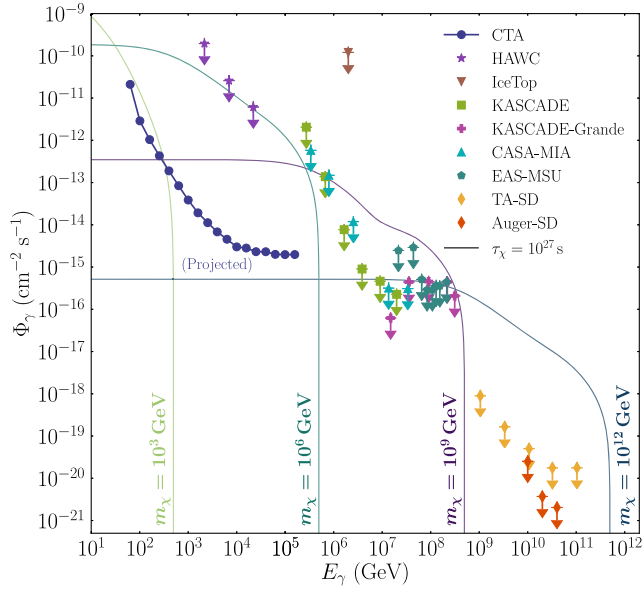
FIG. 1. Expected integral gamma-ray fluxes produced by electroweak corrections to dark matter decay to neutrinos overlaid on the observed gamma-ray distributions. Integral fluxes, defined as the integral of the flux from E_γ to infinity, for four different dark matter masses and lifetime of $\tau_\chi = 10^{27}$ s, are shown as solid lines. Colored symbols indicate observations detailed in the bottom half of Table I.

III. RESULTS

Using the methods outlined above, we present constraints on the DM decay lifetime in Fig. 2. We label the results derived for this work with a heart ($\heartsuit$).

Constraints from neutrino telescopes are shown as shaded regions bordered by solid lines. The overlap in experimental sensitivities yields continuous constraints on the DM lifetime that are much greater than the age of the Universe, ranging from $\tau > 10^{19}$ s at $m_\chi \sim 50$ MeV to $\tau > 10^{27}$ s for $m_\chi \sim 10^{11}$ GeV. The expected neutrino flux on Earth from DM decay is independent of mass. Below $\sim 10^7$ GeV, this is reflected by sensitivity closely following the growth of the electroweak cross section with energy, with some scaling between experiments owing to differences in effective volumes. Above $\sim 10^7$ GeV energies, the Earth becomes opaque to neutrinos, and detection technologies become sensitive to a much smaller solid angle, usually restricted to an area just around the horizon.

Estimated sensitivities of future observatories are shown as dashed lines; these assume five years of data taking. JUNO, Hyper-K, DUNE, KM3NeT, P-ONE, and IceCube-Gen2 should each lead to an improvement of one to two orders of magnitude over current bounds, mainly owing to much larger effective detector volumes. Projected improvements from future radio (GRAND, RNO-G) and modular
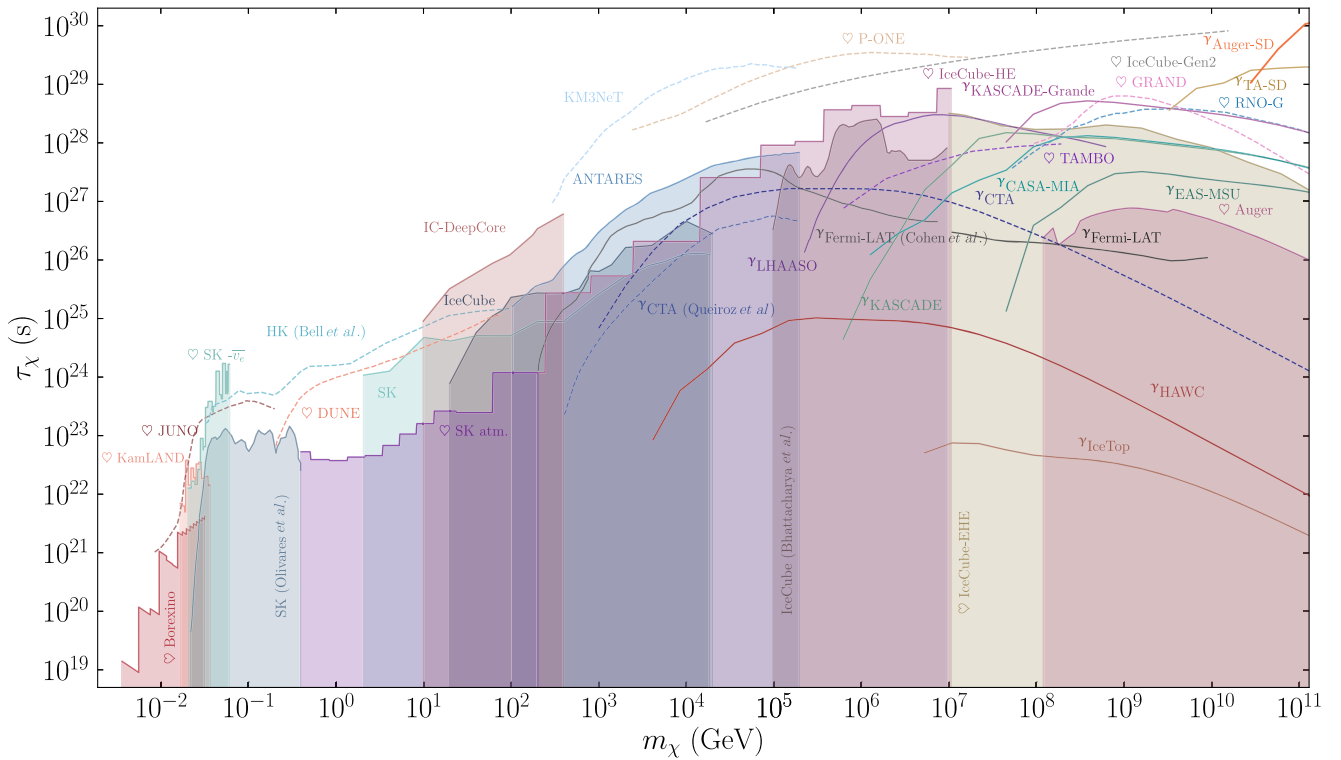

FIG. 2. Constraints on the lifetime of dark matter decaying to neutrinos $\chi \to \bar\nu\nu$. Solid lines bordering shaded regions represent limits from existing neutrino telescope data, solid lines without shading correspond to limits from existing gamma-ray observatories (as shown in Fig. 3), and dashed lines show the reach of future experiments. Labels with a heart symbol correspond to limits derived for this work.
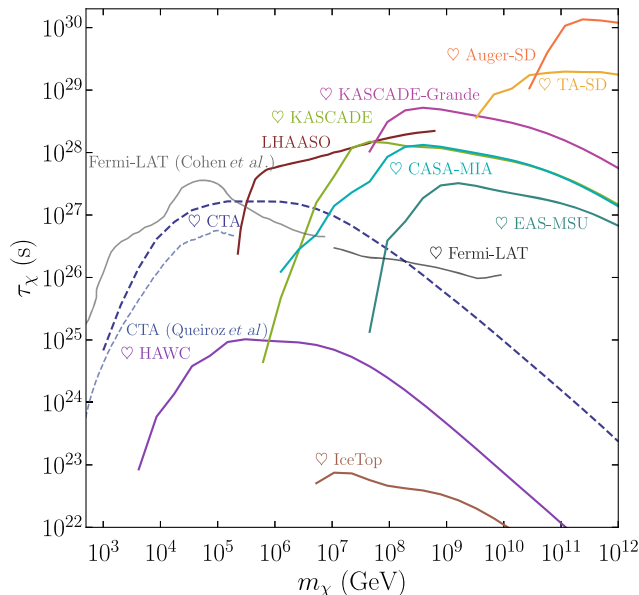
FIG. 3. Gamma-ray constraints on dark matter decay lifetime $\chi \to \bar{\nu}\nu$ due to γ emission from electroweak processes. Solid lines correspond to existing constraints, while the dashed line is a projection for a future experiment. Hearts indicate the new constraints derived in this work. Gamma-ray emission below the electroweak scale is suppressed by powers of M_W [44].

Cherenkov arrays (TAMBO) are more modest, which we mainly attribute to restricted fields of view.

Limits from gamma-ray observatories are marked with a γ superscript. These are also shown separately in Fig. 3. Four experiments dominate the constraints at three different energy ranges. At masses below $\sim 10^5$ GeV, the flux of extragalactic gamma-rays produced by interactions with the IGM is probed by *Fermi*-LAT, yielding the dominant source of gamma-ray constraints in this mass range. At masses between 10^6 and 10^7 GeV, recent measurements by LHAASO supersede prior experiments and improve constraints by nearly four orders of magnitude compared to HAWC. At masses above $10^{7.5}$ GeV, KASCADE-Grande measurements establish the most competitive constraints on the DM decay lifetime limits, outperforming existing neutrino telescopes; at $m_\chi \gtrsim 10^{10}$ GeV, Auger-SD supersedes all other experiments thanks to its monumental effective area. Other experiments considered, such as HAWC or IceTop, remain subdominant over the entire mass range probed here.

IV. FUTURE PROSPECTS & CONCLUSIONS

As shown in Fig. 2, existing neutrino telescopes are able to constrain the lifetime of DM decay to neutrino pairs to values ranging from 10^3 to 10^{12} times the age of the Universe. Upcoming neutrino telescopes will make improvements of one to two orders of magnitude. DUNE and Hyper-Kamiokande will fill in the gap around $m_\chi \sim$ GeV, while the strongest improvements will take place for the next generation of large-volume water and ice Cherenkov telescopes: KM3NeT, P-ONE, and IceCube-Gen2. Though not included here, the ongoing scintillator phase of SNO+ [121] may also shore up constraints on the low-mass end, depending on the timeline for tellurium filling; the inclusion of directional information in, e.g., Borexino [122] or KamLAND analyses could also yield a modest improvement in reach [123,124].

Above the $\sim$TeV range, the electroweak emission of gamma rays opens a new opportunity for discovery, and above 10^8 GeV, gamma rays become the dominant source of information, thanks to the large telescope areas and unsuppressed electroweak emission of photons. What's more the observation of an electromagnetic counterpart will be key in the event of a discovery. Intriguingly, the Square Kilometre Array (SKA) will be sensitive to $\chi \to \bar{\nu}\nu$ [29] in nearby dwarf galaxies for DM masses above a few hundred GeV. Taken together, these observations highlight the importance of multimessenger observations when it comes to elucidating the nature of dark matter.

APPENDIX: SUPPLEMENTARY FIGURES AND TABLES

Here, we include the following tables and figures:
(i) Table II shows the full list of references to datasets or prior analyses used to produce the results of Fig. 2.

TABLE II.   List of datasets used in this work and their references. Left column names the experiment, while the right one provides a short description of the dataset.

Analyses	Data used to derive lifetime limit
ANTARES	Annihilation cross section limit [90]
Auger	Diffuse neutrino flux [48]
Borexino	Upper limit of neutrino flux [49]
DUNE	Annihilation cross section sensitivity [43]
GRAND-200 k	Diffuse neutrino flux sensitivity [47]
Hyper-Kamiokande	Annihilation cross section sensitivity [61]
IceCube	Annihilation cross section limits [50,60]
IC-DeepCore	Annihilation cross section limit [51]
IC (atm.)	Diffuse neutrino flux [52]
IceCube-HE	Diffuse neutrino flux [91,92]
IceCube-EHE	Diffuse neutrino flux [53]
IceCube (Bhattacharya)	Lifetime limit [28]
IceCube-Gen2	Diffuse neutrino flux [93]
JUNO	Lifetime sensitivity [62]
KamLand	Upper limit of neutrino flux [49,54]
KM3NET	Annihilation cross section sensitivity [63]
P-ONE	Projected effective areas [65]
RNO-G	Diffuse neutrino flux sensitivity [64].
SK-$\overline{\nu}_e$	Upper limit of neutrino flux [56]
SK (Olivares)	Annihilation cross section [94]
SK	Annihilation cross section [58]
SK (atm.)	Diffuse neutrino flux [59]
TAMBO	Projected effective areas [66]
IceTop	Upper limit of gamma-ray flux [95]
CTA (Queiroz *et al.*)	Annihilation cross section projection [96]
CTA	Projected γ sensitivity [97]
HAWC	Upper limit of gamma-ray flux [98]
KASCADE	Upper limit of gamma-ray flux [99]
KASCADE-Grande	Upper limit of gamma-ray flux [99]
CASA-MIA	Upper limit of gamma-ray flux [100]
EAS-MSU	Upper limit of gamma-ray flux [101]
TA-SD	Upper limit of gamma-ray flux [102]
Auger-SD	Upper limit of gamma-ray flux [103]

TABLE III.   Exposures and D-factors for experiments discussed in this work. Exposures are converted to RA-dec and averaged over a 24-hour period to obtain the corresponding D-factors, given in units of GeV cm^{-2} sr, and computed according to Eq. (2).

Experiment	Exposure	$D/10^{23}$
All-sky	All-sky	2.65
GRAND	Elevation-dependent exposure, Fig. 24 of [47]	0.298
ANITA	dec = [1.5°, 4°]	0.052
TAMBO	Elevation-dependent exposure, Figs. 3 and 4 of [66]	0.001
	zenith = [90°, 95°]	0.11
Auger	zenith = [75°, 90°]	0.35
	zenith = [60°, 75°]	0.33
	cos(zenith) = [−1, −0.5]	0.83
P-ONE	cos(zenith) = [−0.5, 0.5] [74]	1.35
	cos(zenith) = [0.5, 1]	0.47
	zenith = [90°, 120°]	0.51
ANTARES	zenith = [120°, 150°] [104]	0.46
	zenith = [150°, 180°]	0.29

(Table continued)

TABLE III. *(Continued)*

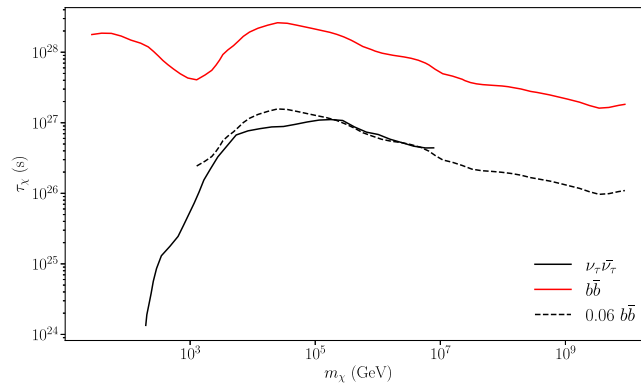| Experiment	Exposure	$D/10^{23}$
IceTop	All-sky	2.63
CTA	Galactic Centre [96]	0.003
HAWC	dec = [−25°–5°]	0.0295
KASCADE	dec = [14°–84°]	0.76
CASA-MIA	dec = [−20°–90°]	1.58
EAS-MSU	dec = [7°–78°]	0.92
TA-SD	zen = [−90°–45°]	1.85

FIG. 4. Demonstration of the scaling from dark matter decay to $b\bar{b}$ constraints to neutrinos. Solid lines show lifetime limits on dark matter decay to $b\bar{b}$ (red) and $\nu_\tau\bar{\nu}_\tau$ (black) as determined by *Cohen et al.* [120] using gamma-ray observation from *Fermi*-LAT. Dashed line shows an approximation for extending the $\chi \rightarrow \nu_\tau\bar{\nu}_\tau$ limits by rescaling the decay to quark limits, by a factor of 0.06, the ratio between total photon production fractions in each channel.
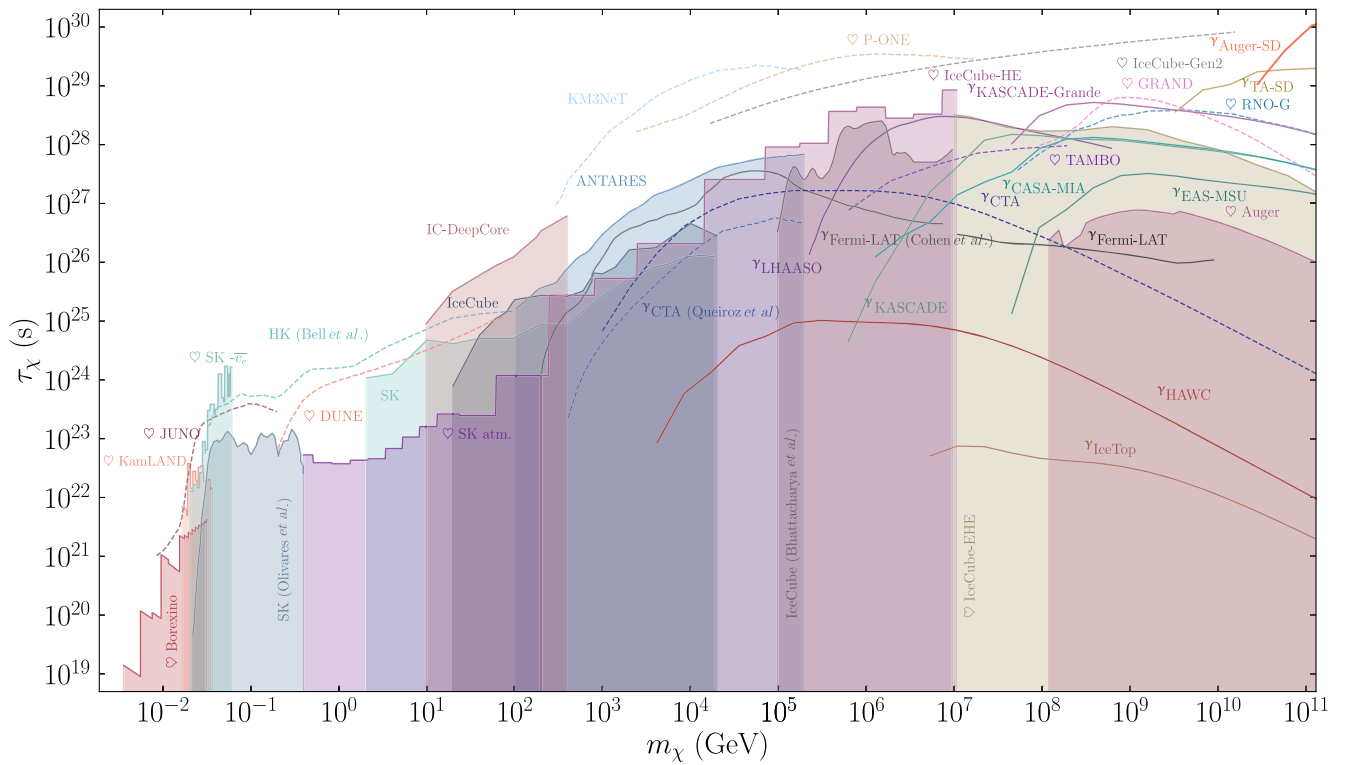

FIG. 5. Larger version of Fig. 2. Solid lines bordering shaded regions represent limits from existing neutrino telescope data, solid lines without shading correspond to limits from existing gamma-ray observatories (as shown in Fig. 3), and dashed lines show the reach of future experiments.

(ii) Table III shows the *D*-factors relevant for each experiment for which we recast diffuse limit fluxes into limits on dark matter decay.

(iii) Figure 4 illustrates the rescaling of *Fermi*-LAT limits on decays to $\bar{b}b$ pairs to limits on $\bar{\nu}\nu$.

(iv) Figure 5 is a larger version of the main results Fig. 2.

---

[1] M. Lisanti, in *New Frontiers in Fields and Strings* (World Scientific, Singapore, 2017), pp. 399–446.

[2] N. Aghanim *et al.* (Planck Collaboration), Astron. Astrophys. **641**, A6 (2020); **652**, C4(E) (2021).

[3] C. Adams *et al.* (MicroBooNE Collaboration), Phys. Rev. D **99**, 092001 (2019).

[4] G. Magill, R. Plestid, M. Pospelov, and Y.-D. Tsai, Phys. Rev. Lett. **122**, 071801 (2019).

[5] A. Stebbins and G. Krnjaic, J. Cosmol. Astropart. Phys. 12 (2019) 003.

[6] R. Harnik, R. Plestid, M. Pospelov, and H. Ramani, Phys. Rev. D **103**, 075029 (2021).

[7] C. A. Argüelles Delgado, K. J. Kelly, and V. Muñoz Albornoz, J. High Energy Phys. 11 (2021) 099.

[8] M. Montero, J. B. Muñoz, and G. Obied, J. High Energy Phys. 11 (2022) 121.

[9] R. Allahverdi, B. Dutta, and K. Sinha, Phys. Rev. D **86**, 095016 (2012).

[10] C. A. Argüelles, V. Muñoz, I. M. Shoemaker, and V. Takhistov, Phys. Lett. B **833**, 137363 (2022).

[11] A. M. Green and B. J. Kavanagh, J. Phys. G **48**, 043001 (2021).

[12] R. Gandhi, C. Quigg, M. H. Reno, and I. Sarcevic, Astropart. Phys. **5**, 81 (1996).

[13] C. A. Argüelles, F. Halzen, L. Wille, M. Kroll, and M. H. Reno, Phys. Rev. D **92**, 074040 (2015).

[14] A. Garcia, R. Gauld, A. Heijboer, and J. Rojo, J. Cosmol. Astropart. Phys. 09 (2020) 025.

[15] J. Alvey and M. Fairbairn, J. Cosmol. Astropart. Phys. 07 (2019) 041.

[16] S. Baumholzer, V. Brdar, P. Schwaller, and A. Segner, J. High Energy Phys. 09 (2020) 136.

[17] C. Boehm, Y. Farzan, T. Hambye, S. Palomares-Ruiz, and S. Pascoli, Phys. Rev. D **77**, 043516 (2008).

[18] M. Escudero, N. Rius, and V. Sanz, J. High Energy Phys. 02 (2017) 045.

[19] Y. Farzan and E. Ma, Phys. Rev. D **86**, 033007 (2012).

[20] Y. Farzan and S. Palomares-Ruiz, J. Cosmol. Astropart. Phys. 06 (2014) 014.

[21] H. H. Patel, S. Profumo, and B. Shakya, Phys. Rev. D **101**, 095001 (2020).

[22] C. Garcia-Cely and J. Heeck, J. High Energy Phys. 05 (2017) 102.

[23] R. Coy and T. Hambye, J. High Energy Phys. 05 (2021) 101.

[24] J. F. Beacom, N. F. Bell, and G. D. Mack, Phys. Rev. Lett. **99**, 231301 (2007).

[25] A. Esmaili, A. Ibarra, and O. L. G. Peres, J. Cosmol. Astropart. Phys. 11 (2012) 034.

[26] C. E. Aisati, M. Gustafsson, and T. Hambye, Phys. Rev. D **92**, 123515 (2015).

[27] C. El Aisati, C. Garcia-Cely, T. Hambye, and L. Vanderheyden, J. Cosmol. Astropart. Phys. 10 (2017) 021.

[28] A. Bhattacharya, A. Esmaili, S. Palomares-Ruiz, and I. Sarcevic, J. Cosmol. Astropart. Phys. 05 (2019) 051.

[29] K. Dutta, A. Ghosh, A. Kar, and B. Mukhopadhyaya, J. Cosmol. Astropart. Phys. 09 (2022) 005.

[30] E. Dudas, L. Heurtier, Y. Mambrini, K. A. Olive, and M. Pierre, Phys. Rev. D **101**, 115029 (2020).

[31] T. N. Maity, A. K. Saha, A. Dubey, and R. Laha, Phys. Rev. D **105**, L041301 (2022).

[32] K. Murase, R. Laha, S. Ando, and M. Ahlers, Phys. Rev. Lett. **115**, 071301 (2015).

[33] K. Murase and J. F. Beacom, J. Cosmol. Astropart. Phys. 10 (2012) 043.

[34] M. Chianese, D. F. G. Fiorillo, R. Hajjar, G. Miele, S. Morisi, and N. Saviano, J. Cosmol. Astropart. Phys. 05 (2021) 074.

[35] M. Chianese, D. F. G. Fiorillo, R. Hajjar, G. Miele, and N. Saviano, J. Cosmol. Astropart. Phys. 11 (2021) 035.

[36] S. Desai *et al.* (Super-Kamiokande Collaboration), Phys. Rev. D **70**, 083523 (2004); **70**, 109901(E) (2004).

[37] K. Abe *et al.* (Super-Kamiokande Collaboration), Phys. Rev. D **102**, 072002 (2020).

[38] M. G. Aartsen *et al.* (IceCube Collaboration), Eur. Phys. J. C **75**, 20 (2015).

[39] M. G. Aartsen *et al.* (IceCube Collaboration), Eur. Phys. J. C **77**, 627 (2017).

[40] R. Abbasi *et al.* (IceCube Collaboration), Phys. Rev. D **105**, 062004 (2022).

[41] R. Abbasi *et al.* (IceCube Collaboration), J. Cosmol. Astropart. Phys. 10 (2023) 003.

[42] L. Heurtier, Y. Mambrini, and M. Pierre, Phys. Rev. D **99**, 095014 (2019).

[43] C. A. Argüelles, A. Diaz, A. Kheirandish, A. Olivares-Del-Campo, I. Safa, and A. C. Vincent, Rev. Mod. Phys. **93**, 035007 (2021).

[44] C. W. Bauer, N. L. Rodd, and B. R. Webber, J. High Energy Phys. 06 (2021) 121.

[45] P. F. de Salas, K. Malhan, K. Freese, K. Hattori, and M. Valluri, J. Cosmol. Astropart. Phys. 10 (2019) 037.

[46] R. Abuter *et al.* (GRAVITY Collaboration), Astron. Astrophys. **615**, L15 (2018).

[47] J. Alvarez-Muniz *et al.* (GRAND Collaboration), Sci. China Phys. Mech. Astron. **63**, 219501 (2020).

[48] E. Zas (Pierre Auger Collaboration), Proc. Sci. ICRC2017 (**2018**) 972.

[49] M. Agostini *et al.* (Borexino Collaboration), Astropart. Phys. **125**, 102509 (2021).

[50] M. G. Aartsen *et al.* (IceCube Collaboration), Eur. Phys. J. C **77**, 627 (2017).

[51] N. Iovine and J. A. Aguilar, arXiv:2107.11224.

[52] M. G. Aartsen *et al.* (IceCube Collaboration), Phys. Rev. D **91**, 122004 (2015).

[53] M. G. Aartsen *et al.* (IceCube Collaboration), Phys. Rev. D **98**, 062003 (2018).

[54] S. Abe *et al.* (KamLAND Collaboration), Astrophys. J. **925**, 14 (2022).

[55] BOREXINO Collaboration, Nature (London) **562**, 505 (2018).

[56] W. Linyan, Experimental studies on low energy electron antineutrinos and related physics, Ph.D. thesis, Tsinghua University, 2018.

[57] A. Olivares-Del Campo, C. BÅ'hm, S. Palomares-Ruiz, and S. Pascoli, Phys. Rev. D **97**, 075039 (2018).

[58] K. Frankiewicz (Super-Kamiokande Collaboration), J. Phys. Conf. Ser. **888**, 012210 (2017).

[59] E. Richard *et al.* (Super-Kamiokande Collaboration), Phys. Rev. D **94**, 052001 (2016).

[60] M. G. Aartsen *et al.* (IceCube Collaboration), Eur. Phys. J. C **76**, 531 (2016).

[61] N. F. Bell, M. J. Dolan, and S. Robles, J. Cosmol. Astropart. Phys. 09 (2020) 019.

[62] K. Akita, G. Lambiase, M. Niibo, and M. Yamaguchi, J. Cosmol. Astropart. Phys. 10 (2022) 097.

[63] S. R. Gozzini, https://pos.sissa.it/358/552/pdf (2019).

[64] J. Aguilar *et al.*, J. Instrum. **16**, P03025 (2021).

[65] M. Agostini *et al.*, Nat. Astron. **4**, 913 (2020).

[66] A. Romero-Wolf *et al.*, arXiv:2002.06475.

[67] G. Bellini *et al.* (Borexino Collaboration), Phys. Lett. B **696**, 191 (2011).

[68] A. Gando *et al.* (KamLAND Collaboration), Astrophys. J. **745**, 193 (2012).

[69] F. An *et al.* (JUNO Collaboration), J. Phys. G **43**, 030401 (2016).

[70] B. Abi *et al.* (DUNE Collaboration), arXiv:2002.03005.

[71] K. Frankiewicz (Super-Kamiokande Collaboration), in *Proceedings, Meeting of the APS Division of Particles and Fields (DPF 2015): Ann Arbor, Michigan, USA, 2015* (2015), arXiv:1510.07999.

[72] K. Abe *et al.* (Super-Kamiokande Collaboration), Phys. Rev. D **102**, 072002 (2020).

[73] ANTARES Collaboration, J. Cosmol. Astropart. Phys. 10 (2015) 068.

[74] M. Agostini *et al.* (P-ONE Collaboration), Nat. Astron. **4**, 913 (2020).

[75] S. Adrian-Martinez *et al.* (KM3Net Collaboration), J. Phys. G **43**, 084001 (2016).

[76] S. Wissel *et al.*, EPJ Web Conf. **216**, 04007 (2019).

[77] M. G. Aartsen *et al.* (IceCube Collaboration), arXiv:1412.5106.

[78] J. Aguilar *et al.*, arXiv:1907.12526.

[79] A. Aab *et al.* (Pierre Auger Collaboration), Nucl. Instrum. Methods Phys. Res., Sect. A **798**, 172 (2015).

[80] W. B. Atwood *et al.*, Astrophys. J. **697**, 1071 (2009).

[81] C. Bigongiari (CTA Consortium Collaboration), Nucl. Part. Phys. Proc. **279–281**, 174 (2016).

[82] A. U. Abeysekara *et al.* (HAWC Collaboration), arXiv:1310.0072.

[83] A. Addazi *et al.* (LHAASO Collaboration), Chin. Phys. C **46**, 035001 (2022).

[84] R. Abbasi *et al.*, Nucl. Instrum. Methods Phys. Res., Sect. A **700**, 188 (2013).

[85] H. O. Klages *et al.*, Nucl. Phys. B, Proc. Suppl. **52**, 92 (1997).

[86] K. G. Gibbs, Nucl. Instrum. Methods Phys. Res., Sect. A **264**, 67 (1988).

[87] Yu. A. Fomin *et al.*, Phys. Rev. D **95**, 123011 (2017).

[88] T. Abu-Zayyad *et al.*, Nucl. Instrum. Methods Phys. Res., Sect. A **689**, 87 (2012).

[89] I. Allekotte *et al.* (Pierre Auger Collaboration), Nucl. Instrum. Methods Phys. Res., Sect. A **586**, 409 (2008).

[90] A. Albert *et al.*, Phys. Lett. B **769**, 249 (2017); **796**, 253(E) (2019).

[91] M. G. Aartsen *et al.*, Astrophys. J. **833**, 3 (2016).

[92] R. Abbasi *et al.* (IceCube Collaboration), Phys. Rev. D **104**, 022002 (2021).

[93] M. Aartsen *et al.* (IceCube Collaboration), arXiv:1911.02561.

[94] A. Olivares-Del Campo, C. Boehm, S. Palomares-Ruiz, and S. Pascoli, Phys. Rev. D **97**, 075039 (2018).

[95] M. G. Aartsen *et al.* (IceCube Collaboration), Astrophys. J. **891**, 9 (2019).

[96] F. S. Queiroz, C. E. Yaguna, and C. Weniger, J. Cosmol. Astropart. Phys. 05 (2016) 050.

[97] G. Maier, L. Arrabito, K. Bernlöhr, J. Bregeon, P. Cumani, T. Hassan, J. Hinton, and A. Moralejo, Proc. Sci. ICRC2019 (**2019**) 733.

[98] A. U. Abeysekara *et al.* (HAWC Collaboration), J. Cosmol. Astropart. Phys. 02 (2018) 049.

[99] W. D. Apel *et al.*, Astrophys. J. **848**, 1 (2017).

[100] M. C. Chantell *et al.*, Phys. Rev. Lett. **79**, 1805 (1997).

[101] Yu. A. Fomin, N. N. Kalmykov, I. S. Karpikov, G. V. Kulikov, M. Yu. Kuznetsov, G. I. Rubtsov, V. P. Sulakov, and S. V. Troitsky, Phys. Rev. D **95**, 123011 (2017).

[102] R. U. Abbasi *et al.* (Telescope Array Collaboration), Astropart. Phys. **110**, 8 (2019).

[103] P. Abreu *et al.* (Pierre Auger Collaboration), J. Cosmol. Astropart. Phys. 05 (2023) 021.

[104] C. Racca (ANTARES Collaboration), in *Frontier Objects in Astrophysics and Particle Physics* (2005), p. 573.

[105] M. G. Aartsen *et al.* (IceCube Collaboration), Phys. Rev. D **91**, 122004 (2015).

[106] M. G. Aartsen *et al.* (IceCube-Gen2 Collaboration), J. Phys. G **48**, 060501 (2021).

[107] M. Honda, M. S. Athar, T. Kajita, K. Kasahara, and S. Midorikawa, Phys. Rev. D **92**, 023004 (2015).

[108] C. A. Argüelles, J. Salvado, and C. N. Weaver, Comput. Phys. Commun. **196**, 569 (2015).

[109] C. A. Argüelles, J. Salvado, and C. N. Weaver, Comput. Phys. Commun. **255**, 107405 (2020).

[110] C. A. Argüelles, J. Salvado, and C. N. Weaver, nuSQuIDS, https://github.com/Arguelles/nuSQuIDS (2015).

[111] R. Acciarri *et al.* (DUNE Collaboration), arXiv:1512.06148.

[112] T. Sjöstrand, S. Ask, J. R. Christiansen, R. Corke, N. Desai, P. Ilten, S. Mrenna, S. Prestel, C. O. Rasmussen, and P. Z. Skands, Comput. Phys. Commun. **191**, 159 (2015).

[113] F. W. Stecker, M. A. Malkan, and S. T. Scully, Astrophys. J. **658**, 1392 (2007).

[114] M. C. Chantell, C. E. Covault, J. W. Cronin, B. E. Fick, L. F. Fortson, J. W. Fowler, K. D. Green, B. J. Newport, R. A. Ong, S. Oser, M. A. Catanese, M. A. K. Glasmacher, J. Matthews, D. F. Nitz, D. Sinclair, J. C. van der Velde, and D. B. Kieda, Phys. Rev. Lett. **79,** 1805 (1997).

[115] Y. A. Fomin, N. N. Kalmykov, I. S. Karpikov, G. V. Kulikov, M. Y. Kuznetsov, G. I. Rubtsov, V. P. Sulakov, and S. V. Troitsky, Phys. Rev. D **95,** 123011 (2017).

[116] S. Cao, Z.-H. Zhu, and N. Liang (LHAASO Collaboration), Phys. Rev. Lett. **129,** 261103 (2022).

[117] A. Franceschini and G. Rodighiero, Astron. Astrophys. **603,** A34 (2017).

[118] B. Skrzypek, M. Chianese, and C. Delgado Argüelles, J. Cosmol. Astropart. Phys. 01 (2023) 037.

[119] K. Murase, J. F. Beacom, and H. Takami, J. Cosmol. Astropart. Phys. 08 (2012) 030.

[120] T. Cohen, K. Murase, N. L. Rodd, B. R. Safdi, and Y. Soreq, Phys. Rev. Lett. **119,** 021102 (2017).

[121] S. Andringa *et al.* (SNO+ Collaboration), Adv. High Energy Phys. **2016,** 6194250 (2016).

[122] M. Agostini *et al.* (BOREXINO Collaboration), Phys. Rev. Lett. **128,** 091803 (2022).

[123] J. R. Klein *et al.*, arXiv:2203.07479.

[124] K. McCormick, APS Phys. **15,** s25 (2022).